Ge-on-Si waveguide photodetectors: multiphysics modeling and experimental validation

Matteo G. C. Alasio*, Michele Goano*†, Alberto Tibaldi*†, Francesco Bertazzi*, Soha Namnabat‡, Donald Adams‡, Prakash Gothoskar‡, Fabrizio Forghieri‡, Giovanni Ghione*, Marco Vallone*
* Dipartimento di Elettronica e Telecomunicazioni, Politecnico di Torino, corso Duca degli Abruzzi 24, 10129 Torino, Italy
† IEIIT-CNR, corso Duca degli Abruzzi 24, 10129 Torino, Italy
‡ Cisco Systems, 7540 Windsor Drive, Suite 412, Allentown, PA 18195, USA
E-mail: michele.goano@polito.it

***Abstract*—This work compares a multiphysics modeling approach with experimental measurements of two Ge-on-Si butt-coupled waveguide photodetectors. The coupled three-dimensional electromagnetic and electrical simulation of the frequency response shows promising agreement with the measurements at 1310 nm, and provides detailed information about significant microscopic quantities, such as the spatial distribution of the optical generation rate.**

I. Introduction

Interconnections between components are one of the bottlenecks in high-speed digital electronics. Silicon photonics (SiPh) [1], [2] enables effective, low-cost optical interconnects, where waveguide photodetectors (WPDs) play a crucial role [3], [4]. Due to their complexity, WPDs require a three-dimensional multiphysics simulation framework [5], [6], describing the optical field propagation from the waveguide to the Ge absorbing region and the transport of the resulting photogenerated carriers. Here we present a preliminary model validation against experimental results of the electro-optic (EO) response [7, Sec. 4.9]. In addition to macroscopic observables, this simulation approach provides the spatial distribution of several microscopic quantities, such as the optical generation rate, which are fundamental towards the detailed understanding and optimization of the device performance.

II. Photodetector structure and modeling approach

The photodetector structure under study is a butt-coupled Ge-on-Si WPD. Two devices with different dimensions have been characterized. Fig.1 shows the geometry used in the simulations, while Table I reports the most relevant geometrical parameters. The photodetector lies over a thin Si substrate, the input optical waveguide being connected with the Si substrate through a taper. The Ge absorption layer is grown on the Si substrate, while the top and lateral metallic contacts allow the WPD to be polarized in reverse bias. A passivation layer of SiO_2 covers and insulates the whole device. In the simulated structures, the Si substrate is highly doped p-type, while Ge is considered intrinsic, with the exception of a n-type region close to the metal/Ge interface with a steep error-function profile. The Ge optical properties are provided by [8], while [9] describes the relevant transport properties, including

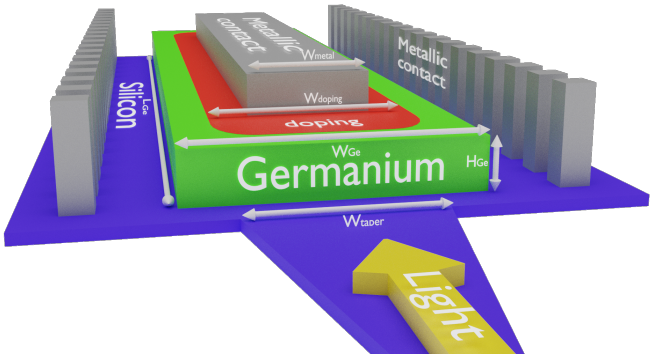

Fig. 1. Perspective view of the photodetector geometry.

models for doping-dependent mobilities and high-field carrier velocity saturation. The Sentaurus TCAD suite by Synopsys [10] provides the platform to perform the multiphysics simulations, generating the mesh, describing the materials parameters and solving the electrical and electromagnetic (EM) problems. Synopsys RSoft FullWAVE [11] uses a finite-difference time-domain (FDTD) solver [12] with a monochromatic wave source to illuminate the device. With respect to [13], the present EM model has been improved by perfectly matched layers (PML) as boundary conditions and a more realistic description of the materials. The optical generation rate distribution $G_{\text{opt}}(x, y, z)$, obtained from the time-averaged Poynting vector extracted from the EM simulation, is used as a source term in the electrical simulations. Sentaurus Device [10] solves the equations of the drift-diffusion model taking into account Fermi-Dirac statistics and incomplete dopant ionization. It considers Shockley-Read-Hall (SRH), radiative, optical generation rate, and Auger processes as generation-recombination terms. Experimental characterization, carried out by Cisco Photonics, involved the measurement of the ratio of the (output) electrical modulation current to the (input) optical modulation power with a Keysight Lightwave Component Analyzer (LCA) [14]. The measurements were performed on two groups of nominally identical devices, five with Device 1 geometry and five with Device 2 geometry (see details in Table I).

978-1-6654-1276-6/21/$31.00 ©2021 IEEE

TABLE I
WPD GEOMETRY

	W_{Ge}	H_{Ge}	L_{Ge}	W_{doping}	W_{metal}	W_{taper}
Device 1	4 μm	0.8 μm	15 μm	3 μm	1.5 μm	2.0 μm
Device 2	2 μm	0.8 μm	15 μm	1.5 μm	1.0 μm	1.5 μm

III. Results, comments and conclusions

Fig. 2 shows comparisons between numerical simulations and measurements of the two devices considered. All results correspond to a reverse bias voltage of 2 V, while the wavelength of the monochromatic source is 1310 nm. The optical power reaching the device is estimated starting from the output power of the laser test source and taking into account the typical losses in the input waveguide. The simulations assume an input optical power $P_{opt} = 200\,\mu$W (-6.98 dBm) at the end of the taper. This is compatible with the input optical power in the device measurements, where the measured laser output power is -1.89 dBm (647 μW), with estimated waveguide losses of 5 dBm. The measurements are from 10 MHz to 50 GHz; some noise is visible above 30 GHz. The experimental estimate of the cutoff frequency reported in Fig. 2 is an average of the measurements over all the nominally identical devices. The simulated and measured cutoff frequencies are in excellent agreement, with an absolute difference of about 2 GHz for Device 2 and even smaller for Device 1. This consistency between simulations and experiments suggests that the multiphysics model may indeed provide a better understanding of the device operation through the study of microscopic quantities such as the spatial distribution of the optical generation rate, that is reported in Fig. 3 as an average over the cross-section of the device along the z light propagation axis.

IV. Acknowledgements

This work was supported in part by Cisco Systems, Inc., under the Sponsored Research Agreement CONCERTI.

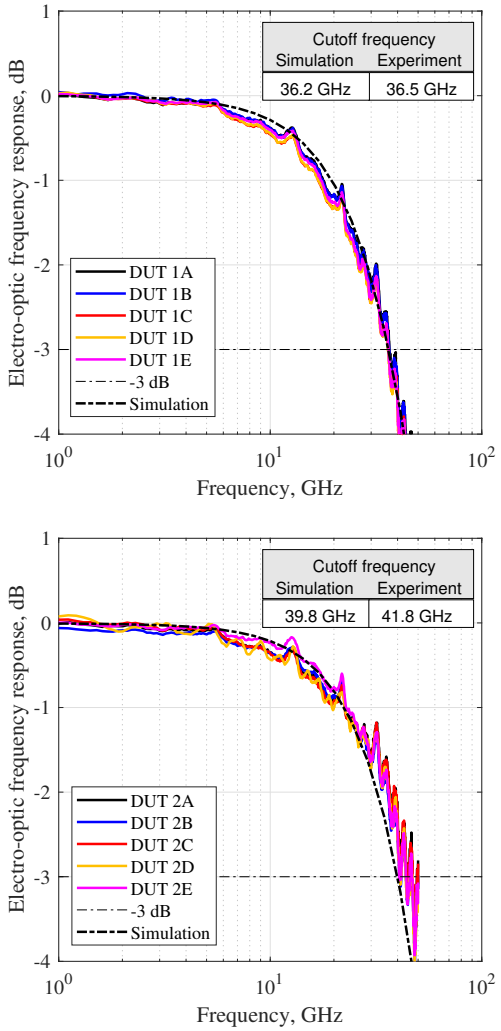

Fig. 2. Simulated and experimental EO frequency response for Device 1 (above) and Device 2 (below).

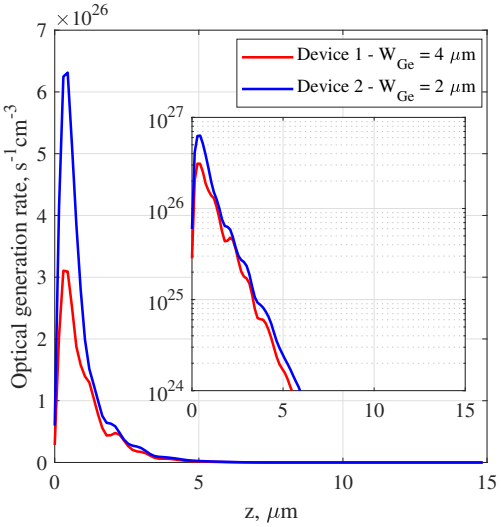

Fig. 3. Optical generation rate in Ge averaged over the WPD cross-section as a function of z.

References

[1] L. Pavesi, D. J. Lockwood, *Silicon Photonics* (Springer-Verlag, Berlin, 2004).
[2] D. J. Lockwood, L. Pavesi, *Silicon Photonics II. Components and Integration* (Springer-Verlag, Berlin, 2011).
[3] D. Thomson, *et al.*, *J. Opt.* **18**, 073003 (2016).
[4] A. H. Atabaki, *et al.*, *Nature* **556**, 349 (2018).
[5] M. M. P. Fard, G. Cowan, O. Liboiron-Ladouceur, *Opt. Express* **24**, 27738 (2016).
[6] A. Palmieri, *et al.*, *20th International Conference on Numerical Simulation of Optoelectronic Devices (NUSOD 2020)* (online, 2020), pp. 27–28.
[7] G. Ghione, *Semiconductor Devices for High-Speed Optoelectronics* (Cambridge University Press, Cambridge, U.K., 2009).
[8] V. Sorianello, *et al.*, *Opt. Mater. Express* **1**, 856 (2011).
[9] A. Palmieri, *et al.*, *Opt. Quantum Electron.* **50**, 71 (2018).
[10] Synopsys, Inc., Mountain View, CA, *Sentaurus Device User Guide. Version N-2017.09* (2017).
[11] Synopsys, Inc., Inc., Optical Solutions Group, Ossining, NY, *RSoft FullWAVE User Guide, v2017.03* (2017).
[12] J.-P. Berenger, *J. Comp. Phys.* **114**, 185 (1994).
[13] M. Vallone, *et al.*, *17th International Conference on Numerical Simulation of Optoelectronic Devices (NUSOD 2017)* (Copenhagen, Denmark, 2017), pp. 207–208.
[14] Keysight Technologies, Santa Rosa, CA, *Lightwave Component Analyzer application notes* (2017).